New Journal of Physics
The open access journal for physics

Efficient carbon ion beam generation from laser-driven volume acceleration

D Jung[1,2,3,5], L Yin[1], B J Albright[1], D C Gautier[1], S Letzring[1], B Dromey[4], M Yeung[4], R Hörlein[3], R Shah[1], S Palaniyappan[1], K Allinger[2], J Schreiber[2,3], K J Bowers[1], H-C Wu[1], J C Fernandez[1], D Habs[2,3] and B M Hegelich[1]

[1] Los Alamos National Laboratory, Los Alamos, NM 87545, USA
[2] Department für Physik, Ludwig-Maximilians-Universität München, D-85748 Garching, Germany
[3] Max-Planck-Institut für Quantenoptik, D-85748 Garching, Germany
[4] Queen's University Belfast, Belfast BT7 1NN, UK
E-mail: djung@lanl.gov

New Journal of Physics **15** (2013) 023007 (10pp)
Received 6 September 2012
Published 5 February 2013
Online at http://www.njp.org/
doi:10.1088/1367-2630/15/2/023007

Abstract. Experimental data on laser-driven carbon C^{6+} ion acceleration with a peak intensity of 5×10^{20} W cm^{-2} are presented and compared for opaque target normal sheath acceleration (TNSA) and relativistically transparent laser–plasma interactions. Particle numbers, peak ion energy and conversion efficiency have been investigated for target thicknesses from 50 nm to 25 μm using unprecedented full spectral beam profile line-out measurements made using a novel high-resolution ion wide-angle spectrometer. For thicknesses of about 200 nm, particle numbers and peak energy increase to 5×10^{11} carbon C^{6+} particles between 33 and 700 MeV (60 MeV u^{-1}), which is a factor of five higher in particle number than that observed for targets with micron thickness. For 200 nm thick targets, we find that the peak conversion efficiency is 6% and that up to 55% of the target under the laser focal spot is accelerated to energies above 33 MeV. This contrasts with the results for targets with micron thickness, where surface acceleration with TNSA is dominant. The experimental findings are consistent with two-dimensional particle-in-cell simulations.

[5] Author to whom any correspondence should be addressed.

Content from this work may be used under the terms of the Creative Commons Attribution-NonCommercial-ShareAlike 3.0 licence. Any further distribution of this work must maintain attribution to the author(s) and the title of the work, journal citation and DOI.

© IOP Publishing Ltd and Deutsche Physikalische Gesellschaft

Contents

1. Introduction

Laser-driven ion acceleration has been investigated for over a decade now [1–7], yet properties of the generated ion beams are still inadequate for applications requiring high ion energies, narrow energy spectra and high conversion efficiency (CE) of laser energy into ion energy. With the target normal sheath acceleration (TNSA) [1, 8], where the laser interacts with an opaque target during the whole pulse duration, proton energies of up to ∼70 MeV [9] have been measured. In TNSA, electrons heated by the laser on the front side penetrate a target that is several microns thick and opaque to the laser during the interaction. A charge separation field is created by these hot electrons on the back of the target due to subsequent field ionization of the target surface; as a result, protons from the surface are accelerated normal to the back of the target. The CE of laser light into protons of the order of 10% [1] has been demonstrated; the typical numbers are 1–2% (e.g. [10, 11]). Acceleration of heavier ions such as carbon is generally inefficient as protons (having the highest charge-to-mass ratio) shield the charge separation field to other ions. Heavier ions are accelerated, but without prior removal of the protons through heating or etching, the CE into heavier species is ∼2 orders of magnitude lower than for protons observed on the same shot. Successful removal of the protons shifts the balance to the next highest charge-to-mass ratio which now exhibits CE at ∼1% level [2, 12]. Energies reach a few MeV u^{-1} [2, 13, 14], which is an order of magnitude too low for ion fast ignition (IFI) [15, 16] and hadron cancer therapy [17]. Recently, numerical experiments using particle-in-cell (PIC) codes on massively parallel supercomputers led to the discovery of radiation pressure acceleration (RPA) [5–7, 18, 19] and the break-out afterburner (BOA) [20–23]. These mechanisms efficiently accelerate all target ions, independent of their charge-to-mass ratio, and promise much higher proton and heavy ion energies. However, they also have more demanding requirements for the laser parameters, such as ultrahigh contrast laser pulses (RPA, BOA), flat top focusing (RPA) and high laser intensities ($>5 \times 10^{19}$ W cm^{-2} for BOA and $>1 \times 10^{22}$ W cm^{-2} for light sail RPA). Those stringent requirements have only allowed first tentative steps toward RPA [24, 25], so far not realizing its full potential. For BOA, on the other hand, a substantial increase in maximum carbon C^{6+} energies has been demonstrated experimentally and progress has been made in manipulating the energy spectra [23, 26, 27]. However, beam properties such as average beam energy, particle numbers or CE have not been researched in detail, either in simulations or in experiments. Detailed knowledge about these parameters is, however, crucial as applications typically have very specific requirements in terms of how many particles are needed at a specific energy.

For carbon IFI, a mono-energetic beam of carbon C^{6+} ions with $E_k \approx 450$ MeV at a maximum bandwidth of 10% and a CE of the order of 10% are necessary [15, 16] (to keep the

laser energy requirements at ∼100 kJ level). For the hadron cancer therapy, protons of 250 MeV or carbon C^{6+} ions of 4–5 GeV are necessary, with particle numbers of the order of 10^9 [17] at the respective energy in a small bandwidth. To keep the laser's advantage of compactness over a conventional synchrotron source, here CE in the 10% range is also desired.

2. Experiment

Here we present a detailed comparison of laser-driven carbon C^{6+} ion acceleration in the BOA and TNSA regimes, including accelerated particle number, average and maximum ion energy and hence the CE, with angularly resolved beam measurements using a novel ion wide-angle spectrometer (iWASP). The data are compared to high-resolution two-dimensional (2D) PIC simulations and to the analytical model published in [19]. The experiments have been carried out at the Trident laser facility [28, 29] with 80 J in 550 fs at a wavelength of 1054 nm and linear polarization (s-pol.). An F/3 off-axis parabolic mirror yields a measured on-target focus of 3.8 μm radius (1/e condition, containing >50% of the laser energy) and a peak laser intensity of $\sim 5 \times 10^{20}$ W cm^{-2} at normal incidence. An exceptionally high laser contrast of the order of 10^{-7} at 4 ps enabled by the optical parametric amplification prepulse eliminator (OPAPE) technique [29] ensures interaction of the laser pulse with a highly overdense plasma [30]. To access both acceleration regimes, synthetic diamond targets with thickness ranging from 50 nm to 25 μm were used, where for the Trident laser parameters BOA is observed to be dominant for thicknesses of < 700 nm, while TNSA is dominant for thicknesses of $\gg 700$ nm. In particular, in BOA the laser energy is dominantly transferred to the ions during the relativistic transparent phase, where $N/\gamma \leqslant 1 < N$ with $N \equiv n_e/n_{cr}$ the normalized target electron density and $n_{cr} = m_e\omega_0^2/(4\pi e^2)$ the critical electron density above which the non-relativistic plasma is opaque to laser light of frequency ω_0 [19]. For thicknesses exceeding 700 nm, the Trident laser energy is insufficient to turn the target relativistically transparent and acceleration gradually turns over to the TNSA regime, i.e. a mostly opaque interaction.

Using an iWASP as described in [31], we were able to measure the carbon C^{6+} energy spectra angularly resolved from -2.5° to 22.5° (with 0° being the laser and target normal) in a line profile horizontal and perpendicular to the laser polarization axis. Figure 1(a) shows the typical angularly resolved carbon ion spectrum of a 200 nm diamond target. The energy resolution is better than 10% at 50 MeV u^{-1} C^{6+}. The iWASP employs only magnetic fields and no electric fields and relies on stopping power for Z-separation (which is largely different for carbon ions and protons) and does not resolve multiple carbon charge states. Nuclear track detectors (Tastrack CR39) [32] are used to measure the carbon signal; the CR39 is covered with 32 μm of Al filtering giving a low-energy cutoff of 33 MeV for carbon ions. Behind the CR39, protons are typically detected with an image plate (data not shown). The pits created by protons with kinetic energy above 11 MeV in the CR39 are not visible with normal etching times and the deflection of protons with less than 11 MeV is large enough so that they do not overlap with carbon ions above 33 MeV, guaranteeing a clean carbon signal on the CR39. Since the iWASP has no electric field, it does not resolve different charge states of carbon ions. Measurements using Thomson parabolas have confirmed that for the laser conditions employed, sub-micron targets are almost fully ionized, and C^{6+} (>90% of carbon ions) and H^+ are the predominant species as shown in [31]; these are well resolved by the iWASP by using a stacked detector consisting of a CR39 for carbon ions and an image plate for protons (see [31] for details). In the thicker target regime ($\gg 700$ nm), where TNSA is dominant, lower carbon charge states are

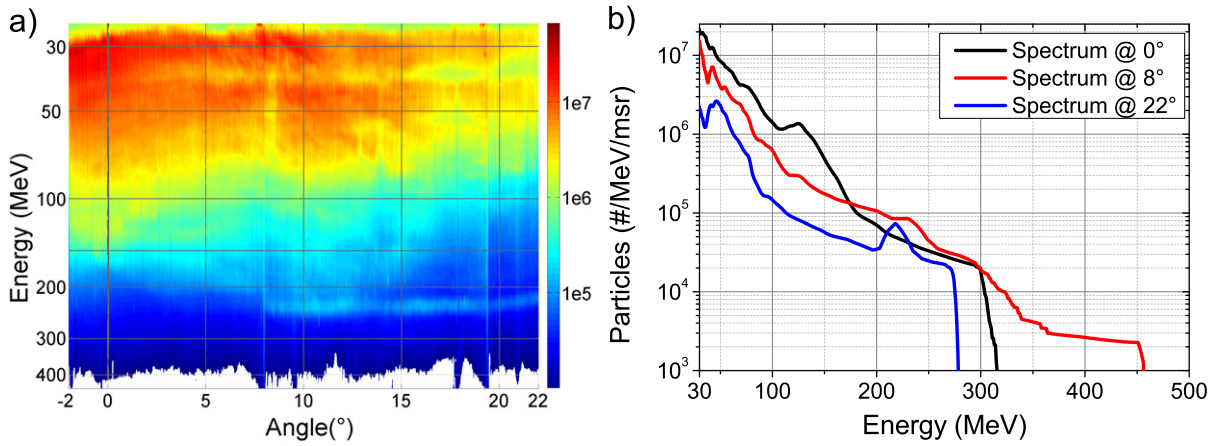

Figure 1. (a) Angularly resolved carbon spectrum measured with the iWASP in the horizontal plane of the ion beam accelerated from a 200 nm diamond target. The laser and target normal is at 0°. (b) Line-outs taken along angles 0°, 8° and 22° from the spectrum displayed in (a). The line-outs mimic spectral measurements of a Thomson parabola at these angles and show for each angle a different high-energy cutoff and different numbers of particles accelerated.

also accelerated and detected from the partially ionized back surface of the target with a C^{6+} abundance of <80% of all carbon ions as estimated from Thomson parabola measurements. This can lead to an overestimate of the particle numbers and CE for thicker targets, since lower charge states, which will be evaluated as C^{6+}, are erroneously attributed higher kinetic energies. To accommodate this, particles numbers below 700 nm are reduced by 10%; for thicker targets, numbers are reduced by 20% as an upper limit.

Despite this caveat, the iWASP offers very accurate measurements of beam parameters such as the maximum energy, the overall number of accelerated particles (and hence the CE), because the solid angle captured by the iWASP is ∼0.4 msr, i.e. up to four orders of magnitude higher than captured by a typical Thomson parabola spectrometer [33, 34]. The benefit of this is shown in figure 1(b); here, spectral line-outs from the spectrum shown in figure 1(a) are shown at angles where commonly measurements with Thomson parabolas are made to retrieve the aforementioned beam parameters. Each spectrum shows a different spectral shape, maximum cutoff energy and different numbers of accelerated particles. Accurate CE measurements based on these spectra would be very difficult to obtain.

To estimate the average ion energy and the particle number of the whole beam, values are first calculated for the measured solid angle (0.4 msr) covering 0–22.5° and are then 'rotated' by 360°, assuming a radially symmetric beam distribution around the target normal with a half-angle of 22.5° corresponding to a solid angle of about 400 msr. This approach is supported by three-dimensional (3D)-VPIC simulations (shown in [35]). The simulations show a very clear rotational symmetry of the ion beam, which is only broken for the highest ion energies, where particle numbers are negligible. The rotational symmetry has also been seen in the experiment; iWASP measurements in directions parallel and perpendicular to the laser polarization axis over many (50+) shots have shown no significant differences in their angular distribution. In particular, for the measurements in the horizontal and vertical planes, the highest particle numbers and particle energies are typically found around 10° off-axis, which is in

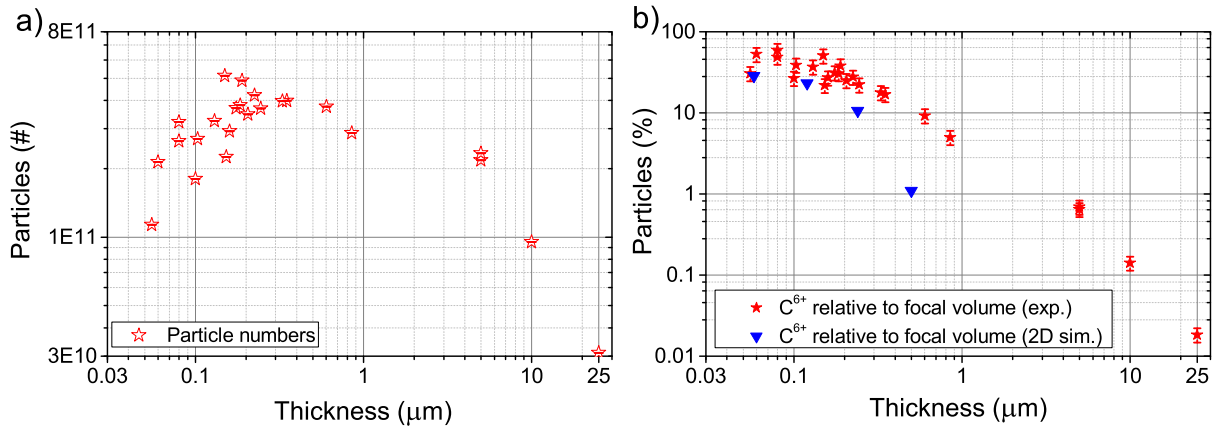

Figure 2. Measured carbon C^{6+} particle numbers above the detection threshold of 33 MeV (a) as a function of target thickness and (b) as a function of laser focal volume for thicknesses of 50 nm to 25 μm encompassing BOA ($<$700 nm) and TNSA ($\gg$700 nm) dominated acceleration regimes. The experimental data are represented by red stars and the simulation results by blue triangles. The laser focal volume is given by the target thickness and the focal spot area (3.8 μm radius for experimental data and $3w$ with $w = 5.12\,\mu$m for simulation data). Errors for particle numbers are derived assuming a Poisson distribution and do not account for systematic errors due to rotational symmetry assumption. Error bars in (b) include uncertainty in the focus diameter.

good agreement with the 3D-VPIC simulations. (These experimental results will be published elsewhere.) It should be noted that with the iWASP, we can capture the irregular radial structure of the ion beam spectra, something that would be difficult with a standard Thomson parabola spectrometer because of its limited solid angle.

In figure 2(a) the measured number of accelerated carbon C^{6+} ions above the detection threshold of the iWASP ($E_{\text{kinetic}} > 33$ MeV) are shown. Note that the error bars only represent the diagnostic lower limit and do not account for systematic errors arising from assuming a rotational symmetry of the ion beam. Carbon particle numbers peak at 5×10^{11}, which corresponds to 35% of the carbon ions contained within the volume of a 180 nm target with area equal to the laser spot of 3.8 μm radius (laser focal volume); for 30 nm, 1 μm and 10 μm target thickness, particle numbers are 1×10^{11}, 3×10^{11} and 1×10^{11} (or 41, 3.5 and 0.125% of the laser focal volume as shown in figure 2(b)). The results from the 180 nm target represent an increase in accelerated particles by a factor of 2–5 relative to the very thin and very thick targets. These results are in good qualitative agreement with 2D-PIC simulations. The blue triangles in figure 2(b) represent particles accelerated to energies above 33 MeV in the simulations for thicknesses ranging from 50 to 500 nm (see section 3 for details); the fraction is given with respect to the target volume under the laser spot area in the simulation, which has a radius of $3w$ ($w = 5.12\,\mu$m).

Although we did not measure the ion beam source size directly, we can use the width of the zeroth order imaged by the slit of the iWASP as an upper bound for the source size. For all thicknesses the image of the slit on the detector followed the projection of a point source, so that we conclude that the source size is comparable to the laser spot size and much smaller than the slit width ($\ll 20\,\mu$m).

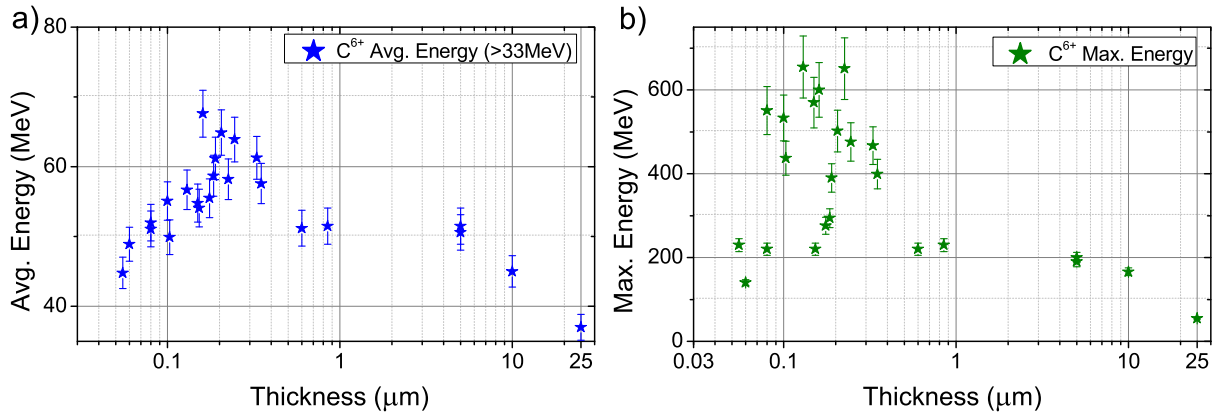

Figure 3. (a) The measured average carbon C^{6+} particle energy above the detection threshold of 33 MeV and (b) the maximum particle energy as a function of target thickness for 50 nm to 25 μm encompassing BOA ($<$700 nm) and TNSA ($\gg$700 nm) dominated acceleration regimes. Error bars are given by the resolution limit of the iWASP (see [31] for details).

Considering that a large fraction of particles has kinetic energies less than 33 MeV (below the spectrometer detection threshold), it is evident that for thin targets where BOA is dominant, essentially all particles from the laser focal volume are accelerated. In particular, for targets with $\gg$700 nm thickness, relative particle numbers drop below 1% of the laser focal volume; at 10 μm, particles would fit into a focal volume of thickness $\sim$10 nm, which agrees well with TNSA dynamics, where particles are being accelerated only from the surfaces (front and back).

At the same time, average particle energies range from 50 MeV in the TNSA to 68 MeV in the BOA regime as depicted in figure 3, which is an increase by a factor of 1.36. This shows that enhanced acceleration for thin sub-μm targets, i.e. within the relativistic transparent regime where BOA is observed to be the dominant acceleration mechanism, is mainly achieved by a volume acceleration of all particles in the laser focal volume, rather than by only accelerating particles from the surfaces as in the TNSA regime.

For the same thickness range, maximum energies increase from $\sim$200 to $\sim$700 MeV, i.e. an increase of 3.5$\times$ (see figure 3(b)). The influence of these high-energy particles on the average energy is negligible, however, due to their lower particle numbers (typically 3–4 orders below particle numbers at the average energy). Hence, high-energy ion 'lobes' possibly breaking the assumed radial symmetry, as discussed in [35], are negligible for the estimates of the average ion energy as well as the CE. The substantially greater scatter in maximum energies is likely a consequence of higher sensitivity to laser and target variability and low particle numbers at these energies close to the detection threshold.

The CE calculated from the particle numbers and the average particle energies is shown in figure 4(a) as a function of target thickness for carbon C^{6+} ions above 33 MeV into a cone with a half-angle of 22.5° (or 400 msr solid angle). Error bars are calculated with standard Gaussian error propagation and give a lower limit of the accuracy given by the detector; errors are most likely higher, especially for thicknesses above 700 nm, as they do not account for systematic errors coming from lower carbon charge states and the assumption of a rotationally symmetric ion beam (as seen in 3D-VPIC simulations). The CE increases toward its maximum of about 6% at a thickness of 200 nm and then decreases until acceleration of carbon ions nearly

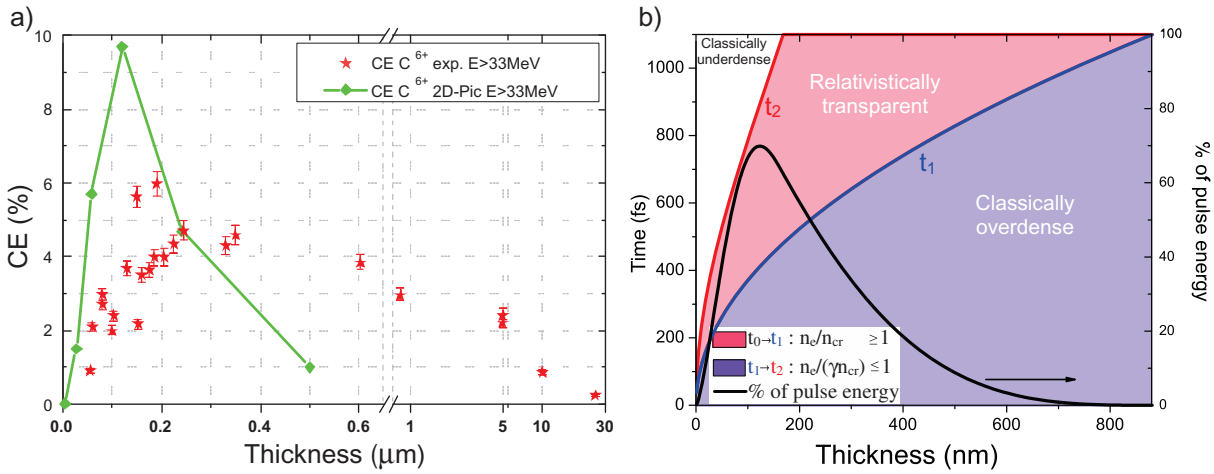

Figure 4. (a) Thickness scaling of the CE as obtained from the experiment with ion energies greater than 33 MeV (red stars) in comparison with 2D-PIC simulation (green squares with E33 MeV). Note that experimentally measured CE for thicknesses $\gg$500 nm are likely to be overestimated, as lower charge states of carbon are more numerous with increasing target thickness and not correctly resolved by the wide-angle spectrometer (see text for details). (b) t_1 (blue solid line) and t_2 (red solid line) as obtained from the analytical model as a function of target thickness for Trident laser parameters. The purple area marks overdense and the red area marks relativistically transparent time of the laser plasma interaction. The white area corresponds to a classically underdense interaction. The fraction of laser energy incident on the target during the relativistic transparency is depicted by the black solid line (pulse duration $\tau = 550$ fs FWHM).

vanishes at 25 μm. The plot shows a linear x-scale (thickness) from 50 to 700 nm where BOA acceleration is dominant and log-scale for thickness $\geqslant$700 nm where TNSA starts to dominate the acceleration. This is an increase by a factor of 2–3 over the CE measured at targets >1 μm and is more than a factor of 5 higher than previously reported [2, 12]. With a CE of about 6%, we are approaching CE requirements for IFI and hadron cancer therapy.

3. Simulation model

In order to further investigate our experimental findings we first compare the results with 2D-PIC simulations. The green solid line/triangles in figure 4(a) show the results of high-resolution 2D-VPIC [36] simulations. The simulation domain is 50×25 μm in the (x, z) plane, and the laser pulse has a time-varying intensity $I(t) = I_0 \sin^2(t\pi/\tau)$ with $I_0 = 5 \times 10^{20}$ W cm^{-2} and $\tau/2$ is the full-width at half-maximum (FWHM) (540 fs, $\lambda = 1054$ nm) and propagates along x. The laser pulse is Gaussian-shaped with the best focus at the target surface with $E_y \sim \exp(-z^2/w^2)$ with $w = 5.12$ μm, close to the experimental conditions. The targets (C^{6+} with 5% protons in number density) are of solid density $N = 821$ (2.8 g cm^{-3}) with a step-function density profile at the beginning of the simulation. Typically, $T_e = 165$ keV and $T_i = 10$ eV for carbon ions and protons, initially; the cell size is $\Delta x = 0.35\lambda_D^0$ (1.2 nm) and $\Delta z = 1.76\lambda_D^0$ (with λ_D^0 the initial

electron Debye length). We use 500, 8210 and 16 420 particles per cell for each species in these simulations (see [35] for a discussion of the effects of initial T_e and the number of simulation particles). The CE has been simulated for targets of 5, 27, 58, 120, 240 and 500 nm target thickness and shows good qualitative agreement with the experimental data in this thickness region. In the PIC simulation, the optimum target thickness is slightly lower, as it does not accurately simulate the pre-expansion of the target due to the slower than $\sin^2$ rise of the real laser pulse; this pre-expansion and hence reduced target density in practice results in an increase of the optimum target thickness as observed in the experiment. Moreover, the size of the simulation box was chosen to give optimum resolution in the BOA regime, but was too small to accurately model TNSA acceleration for the thicker targets, which is why the CE for 500 nm is underestimated by the simulation.

In order to better understand the interaction dynamics in the relativistic transparent regime ($<$700 nm), we take the analytical model presented in [19] and [37], where the acceleration within BOA occurs between the onset of the relativistic transparency at the time t_1 (when the density has decreased to $N/\gamma \approx 1$) and the time t_2 when the target turns classically underdense ($N \approx 1$ and $N/\gamma \ll 1$). t_1 is calculated via a one-dimensional expansion of the target as $t_1 = (12/\pi^2)^{1/4}(N\tau d/(a_0 C_s))^{1/2}$, with a_0 the normalized laser amplitude, d the target thickness and ion sound speed $C_s \approx Q m_e c^2 a_0/m_i$ and charge state Q; t_2 is derived from a 3D isospheric expansion during the relativistic transparency phase as $t_2 = t_1 + Nd(\gamma^{1/3} - 1)/(\gamma C_s \sin(\omega t_1))$, with ω the laser frequency. In figure 4(b), t_1 (blue solid line) and t_2 (red solid line) are plotted as a function of target thickness for Trident parameters (80 J, $\tau = 550$ fs FWHM, $\sin^2$ temporal envelope) with an initial target density of $820 n_{cr}$. The purple area represents laser interacting with an opaque target, while the red area shows interaction with a relativistic transparent target (white area = classically underdense). Strong volumetric heating of electrons across the transparent target and subsequent energy transfer to the ions in the whole focal volume is most efficient when the time of relativistic transparency overlaps with the peak of the laser pulse [37]. This is illustrated by the black solid line, which gives the fraction of laser energy incident on the target between time t_1 and t_2 (as $1/\tau \int_{t_1}^{t_2} \sin^2(t\pi/2\tau)\, dt$). It shows remarkable qualitative agreement with the VPIC results and with the experimental findings at these thicknesses; since the model neglects acceleration for opaque interaction (TNSA) it does not apply to μm-scaled targets for these laser parameters. The maximum laser energy is available for BOA acceleration/relativistic interaction at a thickness of around 200 nm, where experimental data show maximum particle numbers, peak ion energies as well as CE. The experimental data and the t_1–t_2 dynamics presented here suggest that acceleration might be further enhanced by further maximizing the time between t_1 and t_2, i.e. maximizing the available laser energy during the relativistic transparency. Manipulating the expansion of the plasma prior to and during its phase of relativistic transparency could be achieved with a modified laser pulse and/or a special non-uniform target density profile.

4. Summary and conclusion

In conclusion, we presented extensive measurements of carbon ion beam parameters from laser-driven acceleration during opaque (TNSA) and relativistic transparent (BOA) laser–plasma interaction with target thicknesses from 50 nm to 25 μm with enhanced accuracy over prior estimates from the Thomson parabola. The thickness scaling revealed an optimum acceleration in the BOA regime due to a laser interaction with the full target volume within the focal-spot area

with an overall increase in particle numbers and peak ion energies by a factor of 5 with constant laser parameters. The volume acceleration in BOA is an easy tool to accelerate ions other than protons, which is essential for many advanced applications using laser-driven ion beams. For the Gaussian laser pulse shape on Trident, we further observe that the increase in the number of accelerated particles is the dominant source of the CE increase; increases in the average and maximum particle energies are also observed, but contribute less to the overall CE. The high particle numbers of 5×10^{11} and the CE of 6% for carbon ions of >33 MeV are unprecedented and an essential step toward a compact and cost-efficient alternative to conventional accelerator technologies; in particular, the measured peak CE of 6% is close to CE requirements for IFI and hadron cancer therapy. The better knowledge and understanding of the influence of the different interaction regimes on these ion beam parameters will furthermore help to better design laser systems and evaluate the necessary laser parameters for future research.

Acknowledgments

We are grateful for the support by the Trident laser team. The VPIC simulations were run on the LANL Roadrunner supercomputer. The present work was supported by the DOE OFES, Deutsche Forschungsgemeinschaft (DFG) Transregio SFB TR18, Cluster of Excellence (MAP). The work was performed under the auspices of the US Department of Energy by the Los Alamos National Security, LLC, Los Alamos National Laboratory.

References

[1] Snavely R A *et al* 2000 *Phys. Rev. Lett.* **85** 2945–8
[2] Hegelich M *et al* 2002 *Phys. Rev. Lett.* **89** 085002
[3] Mourou G A, Tajima T and Bulanov S V 2006 *Rev. Mod. Phys.* **78** 309–71
[4] Petrov G and Davis J 2009 *Appl. Phys.* B **96** 773–9
[5] Klimo O, Psikal J, Limpouch J and Tikhonchuk V T 2008 *Phys. Rev. Spec. Top.* **11** 031301
[6] Macchi A, Veghini S and Pegoraro F 2009 *Phys. Rev. Lett.* **103** 085003
[7] Esirkepov T, Borghesi M, Bulanov S V, Mourou G and Tajima T 2004 *Phys. Rev. Lett.* **92** 175003
[8] Hatchett S P *et al* 2000 *Phys. Plasmas* **7** 2076–82
[9] Gaillard S A *et al* 2011 *Phys. Plasmas* **18** 056710
[10] Fuchs J *et al* 2006 *Nature Phys.* **2** 48–54
[11] Robinson A P L, Bell A R and Kingham R J 2006 *Phys. Rev. Lett.* **96** 035005
[12] Hegelich B M *et al* 2005 *Phys. Plasmas* **12** 056314
[13] Clark E L, Krushelnick K, Zepf M, Beg F N, Tatarakis M, Machacek A, Santala M I K, Watts I, Norreys P A and Dangor A E 2000 *Phys. Rev. Lett.* **85** 1654–7
[14] McKenna P *et al* 2003 *Phys. Rev. Lett.* **91** 075006
[15] Fernández J C, Honrubia J, Albright B J, Flippo K A, Gautier D C, Hegelich B M, Schmitt M J, Temporal M and Yin L 2009 *Nucl. Fusion* **49** 065004
[16] Honrubia J J, Fernández J C, Temporal M, Hegelich B M and ter Vehn J M 2010 *J. Phys.: Conf. Ser.* **244** 022038
[17] Tajima T, Habs D and Yan X 2009 *Rev. Accel. Sci. Tech.* **2** 201–28
[18] Robinson A P L, Gibbon P, Zepf M, Kar S, Evans R G and Bellei C 2009 *Plasma Phys. Control. Fusion* **51** 024004
[19] Yan X Q, Lin C, Sheng Z M, Guo Z Y, Liu B C, Lu Y R, Fang J X and Chen J E 2008 *Phys. Rev. Lett.* **100** 135003

[20] Yin L, Albright B J, Hegelich B M, Bowers K J, Flippo K A, Kwan T J T and Fernandez J C 2007 *Phys. Plasmas* **14** 056706
[21] Albright B J, Yin L, Bowers K J, Hegelich B M, Flippo K A, Kwan T J T and Fernandez J C 2007 *Phys. Plasmas* **14** 094502
[22] Henig A *et al* 2009 *Phys. Rev. Lett.* **103** 045002
[23] Hegelich B *et al* 2011 *Nucl. Fusion* **51** 083011
[24] Henig A *et al* 2009 *Phys. Rev. Lett.* **103** 245003
[25] Palmer C A J *et al* 2011 *Phys. Rev. Lett.* **106** 014801
[26] Jung D *et al* 2011 *Phys. Rev. Lett.* **107** 115002
[27] Yin L, Albright B J, Jung D, Bowers K J, Shah R C, Palaniyappan S, Fernandez J C and Hegelich B M 2011 *Phys. Plasmas* **18** 053103
[28] Workman J, Cobble J, Flippo K, Gautier D C and Letzring S 2008 *Rev. Sci. Instrum.* **79** 10E905
[29] Shah R C, Johnson R P, Shimada T, Flippo K A, Fernandez J C and Hegelich B M 2009 *Opt. Lett.* **34** 2273–5
[30] Palaniyappan S *et al* 2012 *Nature Phys.* **8** 763–9
[31] Jung D *et al* 2011 *Rev. Sci. Instrum.* **82** 043301
[32] Fleischer R L, Price P B and Walker R M 1965 *J. Appl. Phys.* **36** 3645–52
[33] Thomson J J 1911 *Phil. Mag.* **22** 469–81
[34] Jung D *et al* 2011 *Rev. Sci. Instrum.* **82** 013306
[35] Yin L, Albright B J, Bowers K J, Jung D, Fernández J C and Hegelich B M 2011 *Phys. Rev. Lett.* **107** 045003
[36] Bowers K J, Albright B J, Yin L, Bergen B and Kwan T J T 2008 *Phys. Plasmas* **15** 055703
[37] Yin L, Albright B J, Jung D, Shah R C, Palaniyappan S, Bowers K J, Henig A, Fernndez J C and Hegelich B M 2011 *Phys. Plasmas* **18** 063103